Hosted by Ankara University

Journal of Nuclear Sciences

p-ISSN: 2147-7736, e-ISSN:2148-3981

Journal homepage: http:// jns.ankara.edu.tr

DOI: 10.59474/nuclear.2023.64

Investigation of Radiation Shielding Properties of Pure Iron and Copper-Carbon-Doped Iron Material with GEANT4

E. Tabar[1,*], G. Hoşgör[1], M. R. Ekici[2], C. Aydın[1], İ.N. Muttaki[1]

ORCID: 0000-0002-5093-9409, 0000-0001-5589-9824, 0000-0002-3024-2567, 0009-0009-8259-2305, 0009-0006-8025-4394

[1]Sakarya University, Faculty of Science, Sakarya, Türkiye
[2]Sakarya University, Faculty of Engineering, Metallurgical and Materials Engineering, Sakarya, Türkiye

Received 27.05.2025; received in revised form 04.06.2025; accepted 21.06.2025

ABSTRACT

Pure iron and a Fe-based alloy containing 96 wt.% Fe, 3 wt.% Cu, and 1 wt.% C (hereafter coded as Fe3Cu1C) was fabricated via conventional powder metallurgy. The gamma radiation shielding quantities (linear attenuation coefficient (LAC), mass attenuation coefficient (MAC), half-value layer (HVL), mean free path (MFP), effective atomic number (Zeff), and radiation protection efficiency (RPE)) of pure Fe and Fe3Cu1C were investigated with the Geant4 simulation toolkit within the energy range between 0.04 MeV and 6 MeV. The MAC results were also compared with the XCOM theoretical program. The maximum RPE values were observed at the low energy region between 0.04 and 0.1 MeV, with values of 99.99% (0.04 MeV), 99.63% (0.05 MeV), 96.83% (0.06 MeV), 81.80% (0.08 MeV), and 65.59% (0.10 MeV) for Fe, while 99.99% (0.04 MeV), 99.55% (0.05 MeV), 96.42% (0.06 MeV), 80.68% (0.08 MeV), and 64.26% (0.10 MeV) for Fe3Cu1C. It can be deduced that the results obtained from the present investigation of the Fe3Cu1C material can be used for gamma radiation shielding, especially at low energies.

Keywords: Geant4, Mass attenuation coefficients, Fe, Radiation shielding

1. Introduction

Radiation is critical, particularly in medical diagnostics and treatment. Ionizing radiation can be controlled, detected, and utilized to treat various diseases. However, despite its well-established benefits, radiation exposure must be carefully managed, as excessive or unintended doses pose serious risks to human health [1, 2]. In recent years, glasses and alloys have been investigated as potential materials for radiation protection [3-25]. Alloys have been preferred for internal equipment components, like mobile radiographic systems, industrial non-destructive testing, military applications, and medical equipment, where mechanical strength, thermal stability, and durability precede transparency.

Fe and Fe-based alloys are fundamental materials commonly used for mechanical durability and affordability, especially in construction. Due to its high density, iron (or iron-based alloys) has recently emerged as a viable material for radiation shielding applications. For example, Echeweozo et al. [12] evaluated the gamma radiation shielding endurance of Fe-Nb-Sc alloys doped with Al, Ga, Ge, and Si elements. The results showed that FeNbScGe had the highest mass attenuation coefficient (MAC) values among all investigated alloys. Similarly, Büyükyıldız et al. [13] measured the gamma attenuation of some heavy ferroalloys using the NaI(Tl) detector, and

*Corresponding author.
E-mail address: etabar@sakarya.edu.tr, (E. Tabar)
Journal of Nuclear Sciences, Vol. 9, No.2, December 2022, 23-31

ISSN: 2148-7736

they found notably high MACs. El-Khatib et al. [14] investigated the gamma radiation shielding properties of composites with iron metal dispersed within natural rubber. The results showed that the introduced shielding material can be used for radiation protection. Aygün [15] produced new stainless steel samples with three different contents and investigated the gamma attenuation ability of six different energies. The results showed that the stainless-steel alloys are candidate materials for nuclear applications. Akman et al. [26] studied the gamma radiation attenuation properties of some ternary alloys containing the Fe element, and notable findings were reported.

This study aims to determine the photon shielding performance of pure Fe and Fe3Cu1C alloy. For this purpose, the shielding ability of Fe and Fe3Cu1C was investigated with the Geant4 simulation toolkit within the energy range between 0.04 MeV and 6 MeV, and the results were compared with the XCOM theoretical program.

2. Materials and Methods

2.1 Production of Fe and Fe3Cu1C Alloys with Powder Metallurgy

Fe and Fe3Cu1C (96% Fe, 3% Cu, and 1% C) alloys have been produced by the traditional powder metallurgy technique. Three chemical elements, iron (Fe) (APS: 180 µm, purity: 98%), copper (Cu) (APS: 40-50 µm, purity: 99%), and carbon (C) (APS: 40-50 µm, purity: 99%), were employed in their high-purity powdered form (Nanocar Ltd. Co.). A 50.0 g powder mixture was prepared to produce identical samples. Fe was composed of 100 wt.% Fe and Fe3Cu1C composition was 96 wt.% Fe, 3 wt.% Cu, and 1 wt.% C. For Fe3Cu1C, 48.0 g of Fe, 1.5 g of Cu, and 0.5 g of C were precisely weighed and mixed. The entire batch was homogenized using a ball mill at 200 rpm for 24 hours, using a ball-to-powder mass ratio of 5:1 [11]. Following the milling process, the powder was divided into equal portions (5.0 g each), uniaxially pressed into cylindrical pellets (1.00 cm in diameter, 0.754 cm in thickness), and sintered at 500°C for 1 hour. The density (ρ) of the alloys was measured using Archimedes' principle with distilled water (ρ=1.0 g/cm3) as the immersion liquid, and it was found as 7.167 g/cm3 for pure Fe and 6.904 g/cm3 for Fe3Cu1C. The whole process is represented in Fig. 1.

2.2 Theoretical Background

The mass attenuation coefficient (MAC - μ_m) has been determined using the Beer-Lambert law (Eq. 1) [3, 5-7, 11],

$$\mu_m = \frac{\mu}{\rho} = \frac{\ln\left(\frac{I_0}{I}\right)}{\rho x} \ \text{cm}^2/\text{g} \tag{1}$$

where μ is the linear attenuation coefficient (LAC), I_0 represents the intensity of the incident photons, and I is the intensity of the transmitted photons passing through the materials of different thicknesses (x).

The half-value layer (HVL) (Eq. 2) is defined as the thickness required to reduce radiation levels by 50 % and is calculated as

$$HVL = \frac{\ln 2}{\mu} \ \text{cm} \tag{2}$$

The mean free path (MFP) (Eq. 3) is the average distance a photon travels before interacting with the material.

$$MFP = \frac{1}{\mu} \ \text{cm} \tag{3}$$

The effective atomic number (Z_{eff}) indicates the number of electrons per atom that interact with photons and is given by Eq. 4 [27].

$$Z_{eff} = \frac{\frac{1}{N_A}\sum_i f_i A_i \left(\mu_m\right)_i}{\frac{1}{N_A}\sum_i f_i \frac{A_i}{Z_i}\left(\mu_m\right)_i} = \frac{\sigma_a}{\sigma_{el}} \tag{4}$$

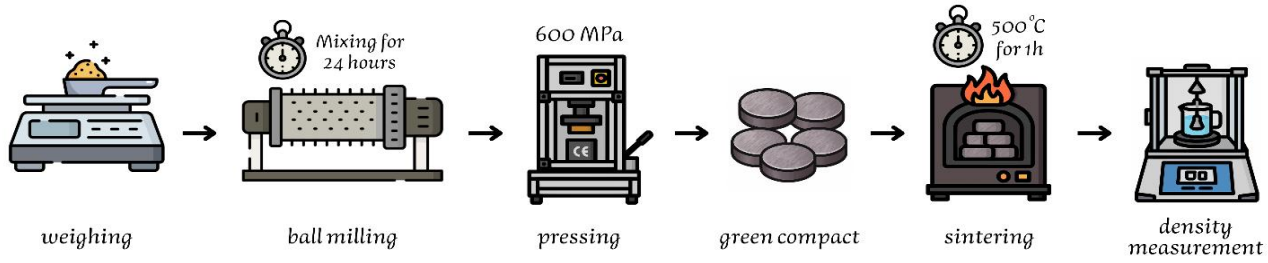

Fig.1 *Schematic representation of the sample preparation process involving weighing, ball milling, pressing, sintering, and measuring density*

To evaluate the radiation shielding performance of the materials, radiation protection efficiency (RPE) (Eq. 5) can be used and defined as

$$RPE(\%) = \left(1 - e^{-\mu x}\right) \times 100 \quad (5)$$

2.3 Monte Carlo simulation codes Geant4 and XCOM theoretical program

To determine the linear attenuation coefficient (LAC) values for Fe and Fe3Cu1C, the GEometry ANd Tracking (Geant4) platform and XCOM: Photon Cross Sections Database [28] were used. The Geant4 view of the simulations, namely Fe and Fe3Cu1C samples as absorbers, a point radioactive source, lead (Pb) collimators to prevent the scattered photons, and a 3×3 inch NaI(Tl) scintillation detector (ORTEC 905-4) are exhibited in Fig. 2. The NaI(Tl) detector was located at a distance of 30 cm from the point of the gamma source. The samples were placed between the source and the NaI(Tl) detector at a distance of 15 cm. A 5.7 cm lead collimator surrounded the NaI(Tl) detector. Before and following the sample, two lead blocks with thicknesses of 5 cm were positioned. A narrow pinhole with a diameter of 0.1 cm was drilled exactly at the center of each block. This configuration was a collimation system to ensure that gamma rays emitted from the point source travel in a straight, well-defined beam path toward the sample. Simulations were performed using 10^6 incident photons for each thickness of the samples (0.1, 0.2, 0.3, and 0.4 cm).

In the Geant4 simulations, the G4EmPenelopePhysics electromagnetic physics list was utilized to model photon interactions accurately across a broad energy range. The Fe3Cu1C alloy was defined using elemental compositions by weight fraction, allowing precise control over material properties and ensuring consistency with their experimental counterparts.

3. Results and Discussions

In this study, the Fe3Cu1C alloy was selected as a candidate material to investigate whether minor additions of Cu and C to Fe can preserve radiation shielding effectiveness while improving mechanical and chemical stability. This composition can offer a safer and more structurally resilient alternative to conventional shielding materials such as lead and concrete.

The gamma radiation shielding performance of Fe and Fe3Cu1C alloy was evaluated using the Geant4 simulation toolkit within the photon energy range of 0.04-6 MeV. For each photon energy, simulations were conducted for four different material thicknesses (0.1, 0.2, 0.3, and 0.4 cm) to obtain transmitted photon counts. The linear attenuation coefficients (LACs), which are inherently dependent only on the material and photon energy, were determined by fitting these counts to the exponential attenuation model. Additionally, to confirm statistical convergence and robustness, selected simulations were repeated using different random seeds, which resulted in negligible variation. These steps validate both the methodological and statistical reliability of the simulation outcomes. An example of the fitted attenuation curve for 0.05 MeV is presented in Fig. 3. This procedure was systematically applied for all energy levels considered in the study.

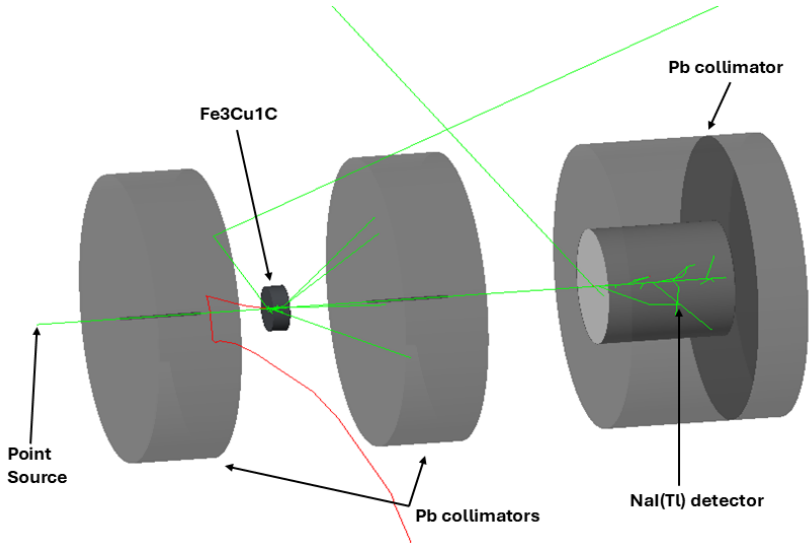

Fig. 2 *Simulation setup for gamma radiation shielding studies. (The dimensions of the NaI(Tl) detector were defined to match its real-world physical specifications. Photomultiplier tube (PMT) was not included. Gamma-ray trajectories are illustrative and do not represent actual photon paths.)*

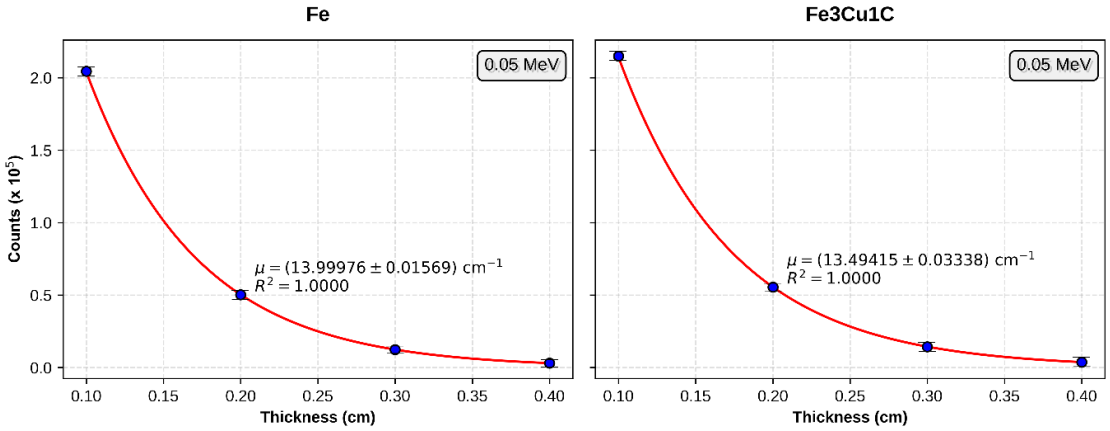

Fig. 3 *Counts (10^5) against material thickness (cm) for Fe and Fe3Cu1C at 0.05 MeV*

MAC values of Fe and Fe3Cu1C alloy obtained by Geant4 simulations and XCOM program with different photon energies are presented in Fig. 4. As shown in Fig. 4, MAC values declined with the increment of photon energies. This trend was consistent with the well-known dominance of the photoelectric effect at lower energies and the progressive contribution of Compton scattering at intermediate energies [29]. The MAC values of the alloys were in between (3.5932±0.0318)-(0.333 ±0.0001) cm^2/g for Fe, and (3.5965±0.0340)-(0.0299±0.0004) cm^2/g for Fe3Cu1C. The maximum MAC values of both alloys were found at 0.04 MeV, and the minimum MACs were at 6 MeV.

Moreover, the MAC values calculated with the XCOM software and simulated with the Geant4 code are listed in Table 1. The relative deviation (RD) between the Geant4 and XCOM results can be calculated by [$RD=((MAC_{XCOM}-MAC_{GEANT4})/MAC_{XCOM})\times100$]. According to Table 1, the calculated differences between XCOM and Geant4 were in between 0.06-3.32% for Fe and 0.01-3.54% for Fe3Cu1C. The difference between the XCOM and Geant4 results was less than 3.54%, and this validated the obtained MAC values. Geant4 (with the Penelope physics list) and XCOM used distinct photon cross-section datasets. Geant4 results were obtained through random Monte Carlo sampling, whereas XCOM values were deterministic. Even with high photon statistics, minor uncertainties may influence the final results. Also, our simulation setup (Fig. 2) approximated ideal collimation and detector response conditions, while XCOM assumed an idealized narrow-beam, infinite-medium geometry. These factors can explain the minor discrepancies that remain within acceptable limits for radiation shielding simulations.

The half-value layer (HVL) and mean free path (MFP) values for Fe and Fe3Cu1C are presented in Table 2. The HVL and MFP values depended on photon energies and increased as photon energies increased. For instance, at

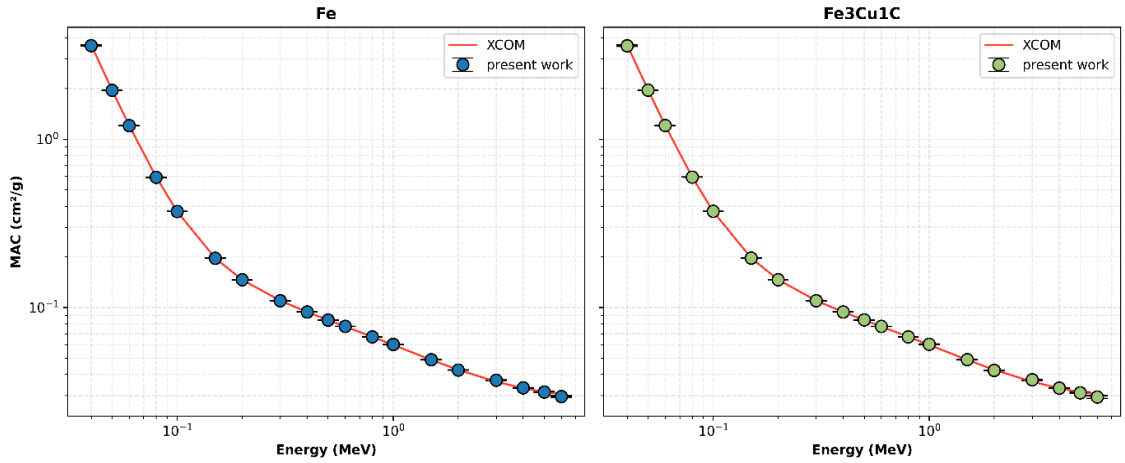

Fig. 4 *The mass attenuation coefficient (MAC) of Fe (left) and Fe3Cu1C (right) against energy. The red solid line represents the theoretical results obtained from XCOM. Error bars have been added to the simulation data to indicate statistical uncertainties*

Table 1. Mass attenuation coefficients (MAC) obtained by the Geant4 simulation and XCOM program, with the deviation between the two methods for Fe and Fe3Cu1C

Energy (MeV)	Fe			Fe3Cu1C		
	Geant4	XCOM	RD (%)	Geant4	XCOM	RD (%)
0.04	3.5932±0.0318	3.629	0.99	3.5916±0.0354	3.632	1.11
0.05	1.9534±0.0022	1.957	0.19	1.9545±0.0048	1.959	0.23
0.06	1.2039±0.0018	1.205	0.09	1.2061±0.0014	1.206	0.01
0.08	0.5943±0.0011	0.5952	0.14	0.5953±0.0010	0.5959	0.10
0.10	0.3721±0.0003	0.3717	0.12	0.3726±0.0002	0.3721	0.13
0.15	0.1963±0.0005	0.1964	0.06	0.1964±0.0005	0.1966	0.08
0.20	0.1461±0.0002	0.1460	0.09	0.1463±0.0002	0.1461	0.11
0.30	0.1097±0.0003	0.1099	0.17	0.1098±0.0002	0.1099	0.05
0.40	0.0941±0.0001	0.094	0.15	0.0941±0.0001	0.09402	0.09
0.50	0.0843±0.0001	0.08415	0.22	0.0844±0.0001	0.08416	0.23
0.60	0.0773±0.0000	0.07704	0.34	0.0772±0.0001	0.07705	0.26
0.80	0.0669±0.0000	0.06699	0.15	0.0669±0.0001	0.067	0.22
1.00	0.0603±0.0002	0.05995	0.61	0.0605±0.0002	0.05996	0.83
1.50	0.0489±0.0002	0.04883	0.12	0.0490±0.0003	0.04884	0.38
2.00	0.0425±0.0001	0.04265	0.47	0.0423±0.0002	0.04265	0.71
3.00	0.0370±0.0001	0.03621	2.12	0.0372±0.0003	0.0362	2.81
4.00	0.0333±0.0001	0.03312	0.57	0.0332±0.0001	0.03309	0.32
5.00	0.0315±0.0002	0.03146	0.13	0.0311±0.0002	0.03143	1.15
6.00	0.0296±0.0003	0.03057	3.32	0.0294±0.0006	0.03053	3.54

Table 2. The half-value layer (HVL) and mean free path (MFP) obtained by the Geant4 simulation for pure Fe and Fe3Cu1C alloy

Energy (MeV)	Fe		Fe3Cu1C	
	HVL (cm)	MFP (cm)	HVL (cm)	MFP (cm)
0.04	0.0269	0.0388	0.0317	0.0457
0.05	0.0495	0.0714	0.0582	0.0840
0.06	0.0803	0.1159	0.0943	0.1361
0.08	0.1627	0.2348	0.1911	0.2757
0.10	0.2599	0.3750	0.3053	0.4404
0.15	0.4927	0.7108	0.5791	0.8355
0.20	0.6620	0.9550	0.7775	1.1216
0.30	0.8816	1.2719	1.0359	1.4945
0.40	1.0278	1.4828	1.2087	1.7438
0.50	1.1473	1.6551	1.3477	1.9443
0.60	1.2511	1.8050	1.4733	2.1256
0.80	1.4456	2.0856	1.7002	2.4529
1.00	1.6039	2.3139	1.8800	2.7123
1.50	1.9778	2.8533	2.3213	3.3489
2.00	2.2756	3.2830	2.6889	3.8793
3.00	2.6139	3.7710	3.0576	4.4112
4.00	2.9043	4.1900	3.4260	4.9426
5.00	3.0703	4.4295	3.6573	5.2764
6.00	3.2674	4.7138	3.8688	5.5815

0.08 MeV, the HVL and MFP values were 0.1627 cm and 0.2348 cm for Fe and 0.1911 cm and 0.2757 cm for Fe3Cu1C, respectively. At 1.5 MeV, these values rose to 1.9778 cm (HVL) and 2.8533 cm (MFP) for Fe, and 2.3213 cm and 3.3489 cm for Fe3Cu1C. Across all energies, the Fe3Cu1C alloy exhibited higher HVL and MFP values than pure Fe, indicating its relatively lower photon attenuation efficiency.

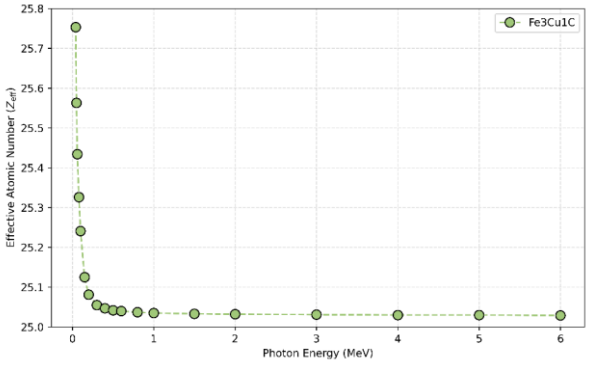

Fig. 5 *The effective atomic number (Z_{eff}) of the Fe3Cu1C alloy*

Fig. 5 shows the difference in effective atomic number (Z_{eff}) in the gamma energy spectrum of 0.04-6 MeV for Fe3Cu1C alloys. For pure Fe, it was found as Z_{eff} =26. The Z_{eff} values of Fe3Cu1C lied in between 25.753 and

25.029. Compared to pure Fe, a slightly reduced Z_{eff} value was observed for Fe3Cu1C that indicated a decreased ability for photon interaction, especially in the lower energy range where the photoelectric effect was the most significant. This reduction can be attributed to incorporating the low-*Z* element, carbon, into the alloy. However, the difference was minimal enough that the overall attenuation performance remained comparable to the pure iron.

Fig. 6 illustrates the radiation protection efficiency (RPE) of Fe and Fe3Cu1C alloy as a function of the energies in a 0.4 cm thickness. RPE values were in between 99.9966-8.1242% for pure Fe and 99.9951-0.9219% for Fe3Cu1C. In summary, a 0.4 cm thick pure Fe at 0.04 MeV energy can stop 99.66% of incoming gamma photons, while the Fe3Cu1C alloy can stop 99.55% of incoming photons.

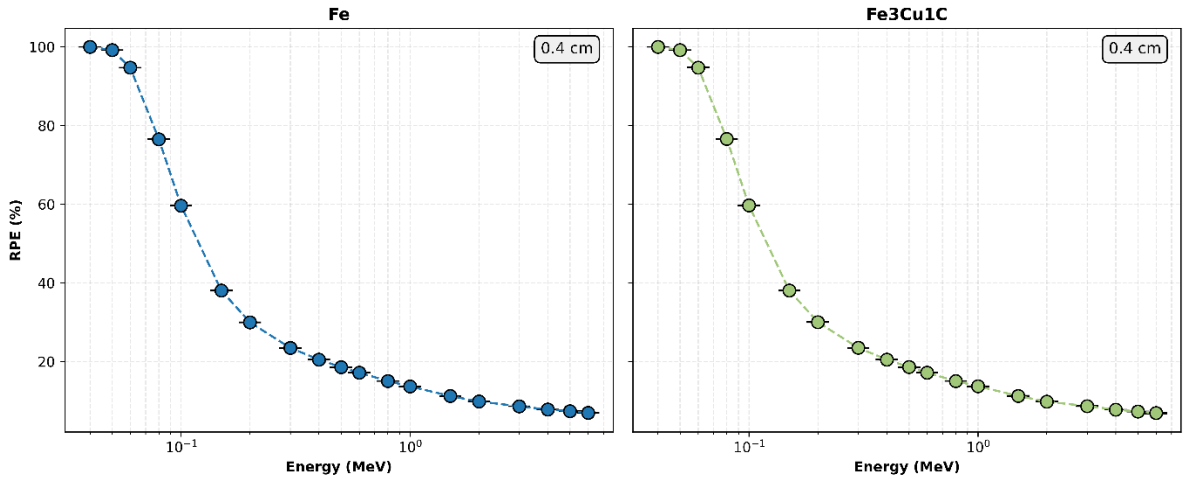

Fig. 6 *Radiation Protection Efficiency (RPE) of Fe (left) and Fe3Cu1C (right) at a fixed sample thickness of 0.4 cm as a function of photon energy. Error bars represent the statistical uncertainties associated with the simulation results*

In Fig. 7, the MAC values of Fe and Fe3Cu1C were compared with some other Fe-based alloys at 0.08 MeV. Fe (0.5943 cm^2/g) and Fe3Cu1C (0.5953 cm^2/g) had higher MAC values than Fe/Cr18/Ni10 (0.5605 cm^2/g), Fe/Cr21/Ni32.5 (0.5860 cm^2/g), Fe/Cr25/Ni20 (0.570 cm^2/g), and Fe/Cr17/Ni72 (0.5511 cm^2/g) [26]. On the other hand, the alloys named Fe/Cr16/Ni72 (0.6522 cm^2/g) [26], FeNbScAl (1.0315 cm^2/g), FeNbScGa (1.0770 cm^2/g), FeNbScGe (1.0934 cm^2/g), FeNbScSi

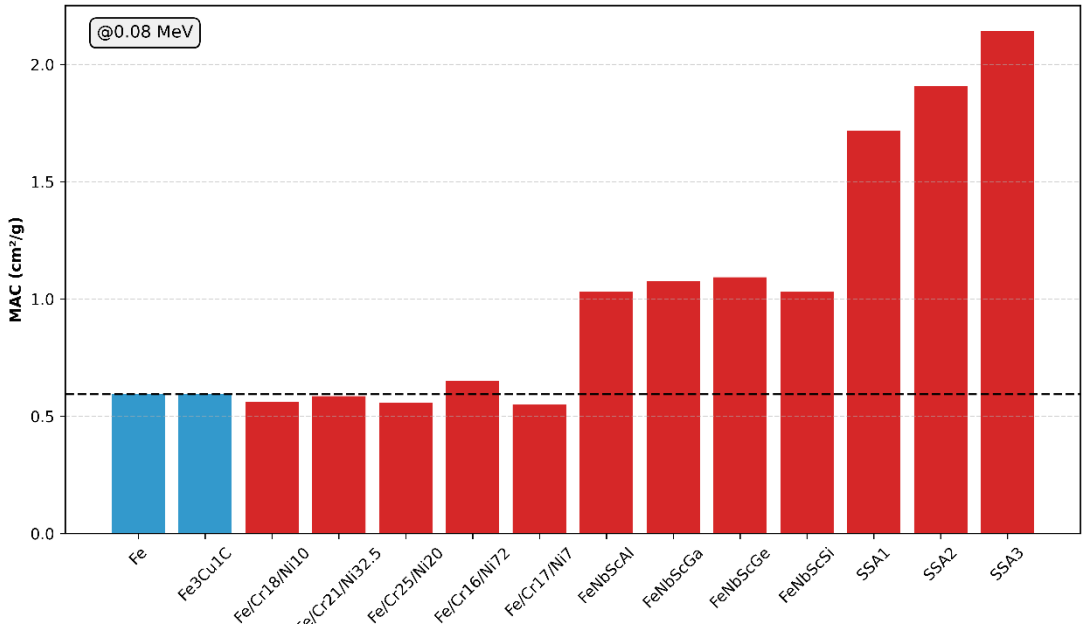

Fig. 7 *Comparison of the MAC (cm^2/g) values for pure Fe and Fe3Cu1C alloy (blue columns) with other Fe-doped alloys and materials (red columns)*

(1.0301 cm^2/g) [12], SSA1 (1.719 cm^2/g), SSA2 (1.909 cm^2/g), SSA3 (2.144 cm^2/g) [15] had higher MAC values than Fe and Fe3Cu1C. FeNbSc-based alloys [12], particularly those containing heavier elements such as Nb, Ga, and Ge, exhibited substantially higher MAC values than Fe3Cu1C. This suggested that incorporating elements with higher atomic numbers (*Z*) can significantly improve gamma-ray attenuation. Moreover, the SSA alloy series [15], which contained high-*Z* elements such as W, Mo, and Re, showed the highest attenuation performance among all samples analyzed.

Conclusion

This work evaluated the gamma radiation shielding performance of Fe and Fe3Cu1C alloy using the Geant4 simulation toolkit within the different photon energies. The linear attenuation coefficients (LACs), mass attenuation coefficients (MACs), half-value layers (HVLs), mean free paths (MFPs), effective atomic number (Zeff), and radiation protection efficiency (RPE) were calculated, and the MAC results were compared with the XCOM theoretical data and some other Fe-doped materials. The difference between the XCOM and Geant4 results was less than 3.54%, and this validated the obtained MAC values. The prepared Fe3Cu1C alloy radiation shielding performed better than the other Fe-doped materials (Fe/Cr18/Ni10, Fe/Cr21/Ni32, Fe/Cr25/Ni20, and Fe/Cr17/Ni72). Compared to pure iron (Fe), the slightly lower effective atomic number (Zeff) observed in the Fe3Cu1C alloy indicated a reduced ability for photon interaction, particularly in the lower energy range where the photoelectric effect was the most significant. This reduction was attributed to incorporating a low-Z element, carbon, into the alloy.

Although the Fe3Cu1C alloy exhibited a slightly lower radiation attenuation capacity than pure iron, it may offer advantages in other aspects. Carbon can increase hardness and tensile strength by promoting solid solution and carbide formation [30]. At the same time, copper can improve corrosion resistance and atmospheric durability in iron-based alloys [31]. While these effects were not experimentally evaluated in the present study, such enhancements could render Fe3Cu1C a more suitable candidate for radiation shielding applications requiring structural strength or environmental stability.

Conflict of Interest

The authors have no conflict of interest.

Acknowledgments

This study was supported by 2209-A University Students Research Projects Support Program.

References

[1] A.S. Abouhaswa, Y.S. Rammah, M.I. Sayyed, and H.O. Tekin, "Synthesis, structure, optical and gamma radiation shielding properties of B2O3-PbO2-Bi2O3 glasses", Composites Part B: Engineering 172 218-225 (2019).

[2] A.S. Abouhaswa, H.M.H. Zakaly, S.A.M. Issa, M. Pyshkina, R. El-Mallawany, and M.Y.A. Mostafa, "Lead borate glasses and synergistic impact of lanthanum oxide additive: optical and nuclear radiation shielding behaviors", Journal of Materials Science: Materials in Electronics 31(17) 14494-14501 (2020).

[3] Z. Hoşgör, M. Ünlütürk, S. Gülmez, Ü. Anıl, S. Yazan, G. Hoşgör, and E. Tabar, "Effect of SnO2 on material and radiation shielding properties in SiO2-B2O3-Na2O-K2O-ZnO glass system ", Ceramics International (accepted) (2025).

[4] M.I. Sayyed, M.H.A. Mhareb, B.C. Şakar, K.A. Mahmoud, E. Şakar, et al., "Experimental investigation of structural and radiation shielding features of Li2O-BaO-ZnO-B2O3-Bi2O3 glass systems", Radiation Physics and Chemistry 218 111640 (2024).

[5] M.R. Ekici, T. Emre, Y. Ramazan, H. Gamze, and E. and Bulut, "Investigation of the Effects of Magnesium, Iron, and Manganese on Gamma Permeability in Zinc-Based Alloys Produced by Powder Metallurgy", Nuclear Technology 1-17 (2025).

[6] G. Hoşgör and E. Tabar, "The investigation of the radiation shielding features of boro-tellurite glasses containing bismuth and titanium via FLUKA code", Physica Scripta 100(1) 015308 (2025).

[7] G. Hoşgör, E. Tabar, E. Kemah, and H. Yakut, "Influence of TiO2 content on the radiation shielding properties of the La2O3-B2O3-Gd2O3-Nb2O5-ZrO2-SiO2 glasses", Radiation Physics and Chemistry 226 112281 (2025).

[8] A. Acikgoz, I. Izguden, Y. Tasgin, D. Yilmaz, G. Demircan, S. Kalecik, and B. Aktas, "Influence of praseodymium oxide on the structural, mechanical and photon, charged particles, and neutron shielding properties of alumina borate glass", Ceramics International 50(19, Part A) 34573-34584 (2024).

[9] Y. Al-Hadeethi, M.I. Sayyed, and S.A. Tijani, "Gamma radiation attenuation properties of tellurite glasses: A comparative study", Nuclear Engineering and Technology 51(8) 2005-2012 (2019).

[10] M.S. Al-Buriahi, I.O. Olarinoye, S. Alomairy, I. Kebaili, R. Kaya, H. Arslan, and B.T. Tonguc, "Dense and environment friendly bismuth barium telluroborate

glasses for nuclear protection applications", Progress in Nuclear Energy 137 103763 (2021).

[11] M.R. Ekici, E. Tabar, G. Hoşgör, E. Bulut, and A. Atasoy, "The effect of zinc, iron and manganese content on gamma shielding properties of magnesium-based alloys produced using the powder metallurgy", Nuclear Engineering and Technology 56(9) 3872-3883 (2024).

[12] E.O. Echeweozo, A. Norah, A. Sultan, A.Z. A., A.N. Salem, and M.S. and Al-Buriahi, "Evaluation of gamma radiation shielding characteristics of FeNbSc-based alloys", Radiation Effects and Defects in Solids 1-16 (2025).

[13] M. Büyükyıldız, S. Thakur, A. Levet, and P. Kaur, "Gamma-ray attenuation properties of some heavy metal ferroalloys for potential applications", Progress in Nuclear Energy 176 105382 (2024).

[14] A.M. El-Khatib, A.S. Doma, M.M. Abbass, M.F. Hassan, M.I. Abbas, M.M. Abd El-Latif, and M.M. Gouda, "Enhancing gamma radiation shielding properties of iron metal and natural rubber composites", Journal of Applied Polymer Science 141(30) e55690 (2024).

[15] B. Aygün, "High alloyed new stainless steel shielding material for gamma and fast neutron radiation", Nuclear Engineering and Technology 52(3) 647-653 (2020).

[16] F. Akman, M.I. Sayyed, M.R. Kaçal, and H.O. Tekin, "Investigation of photon shielding performances of some selected alloys by experimental data, theoretical and MCNPX code in the energy range of 81 keV–1333 keV", Journal of Alloys and Compounds 772 516-524 (2019).

[17] R. Darwesh, M.I. Sayyed, Y. Al-Hadeethi, and J.S. Alotaibi, "Synthesis and characterization of TeO2-B2O3-CaO-ZnO glass systems for improved radiation shielding performance", Journal of Radiation Research and Applied Sciences 18(1) 101259 (2025).

[18] B.B. Solak, B. Aktas, D. Yilmaz, S. Kalecik, S. Yalcin, A. Acikgoz, and G. Demircan, "Exploring the radiation shielding properties of B2O3-PbO-TeO2-CeO2-WO3 glasses: A comprehensive study on structural, mechanical, gamma, and neutron attenuation characteristics", Materials Chemistry and Physics 312 128672 (2024).

[19] M.H. Alhakami, A.S. Abouhaswa, N.A. Althubiti, and T.A.M. Taha, "Investigation of optical and radiation shielding properties in bismuth oxide-doped barium borate glasses", Nuclear Engineering and Technology 57(9) 103633 (2025).

[20] R. Kurtulus, "Recent developments in radiation shielding glass studies: A mini-review on various glass types", Radiation Physics and Chemistry 220 111701 (2024).

[21] H. Özdoğan, F. Akman, Ö. Kilicoglu, Y. Gökçe, and Y.A. Üncü, "Monte Carlo simulation study on the radiation attenuation characteristics of doxorubicin-treated femur and tibia bones in rats", Radiation Physics and Chemistry 235 112841 (2025).

[22] H. Özdoğan, Y.A. Üncü, F. Akman, H. Polat, and M.R. Kaçal, "Detailed Analysis of Gamma-Shielding Characteristics of Ternary Composites Using Experimental, Theoretical and Monte Carlo Simulation Methods", Polymers 16(13) 1778 (2024).

[23] Y. Gökçe, F. Akman, Ö. Kılıçoğlu, Y. Ali Üncü, and H. Özdoğan, "Monte Carlo simulation analysis of radiation attenuation properties induced by arsenic accumulation in femur and tibia bones of rats exposed to sodium arsenite diet", Radiation Physics and Chemistry 225 112114 (2024).

[24] Y. Gökçe, F. Akman, Ö. Kılıçoğlu, Y.A. Üncü, and H. Özdoğan, "A pilot study of diabetes effects on radiation attenuation characteristics of tibia and femur of rats", Applied Radiation and Isotopes 208 111296 (2024).

[25] Y.A. Üncü, G. Sevim, O. Ağar, and H. Özdoğan, "Mass attenuation coefficient, stopping power, and penetrating distance calculations via Monte Carlo simulations for cell membranes", Kuwait Journal of Science 50(1A) (2023).

[26] F. Akman, M.R. Kaçal, M.I. Sayyed, and H.A. Karataş, "Study of gamma radiation attenuation properties of some selected ternary alloys", Journal of Alloys and Compounds 782 315-322 (2019).

[27] E.E. Saleh, M.A. Algradee, A.M. Qaid, and D.a.A. Taya, "Cd–S doped glass Shields: Structural, optical, and nuclear shielding characteristics", Radiation Physics and Chemistry 237 112969 (2025).

[28] M. Berger, J.H. Hubbell, S. Seltzer, J. Chang, J. Coursey, et al. XCOM: Photon Cross Sections Database. https://www.nist.gov/pml/xcom-photon-cross-sections-database 2025.

[29] O. Agar, E. Kavaz, E.E. Altunsoy, O. Kilicoglu, H.O. Tekin, et al., "Er2O3 effects on photon and neutron shielding properties of TeO2-Li2O-ZnO-Nb2O5 glass system", Results in Physics 13 102277 (2019).

[30] R.S. Sundar and S.C. Deevi, "Effect of carbon addition on the strength and creep resistance of FeAl alloys", Metallurgical and Materials Transactions A 34(10) 2233-2246 (2003).

[31] S.O. Seidu, S.S. Owoeye, and H.T. Owoyemi, "Assessing the effect of copper additions on the corrosion behaviour of grey cast iron", Leonardo Electronic Journal of Practices and Technologies 14(26) 49-58 (2015).